J|A|C|S
ARTICLES
Published on Web 10/19/2004

Evidence for Through-Space Electron Transfer in the Distance Dependence of Normal and Inverted Electron Transfer in Oligoproline Arrays

Scafford A. Serron, W. Stephen Aldridge III, Cavan N. Fleming, Ryan M. Danell, Mu-Hyun Baik, Milan Sykora, Dana M. Dattelbaum, and Thomas J. Meyer*,§

Contribution from the Department of Chemistry, University of North Carolina at Chapel Hill, CB # 3290, Chapel Hill, North Carolina 27599-3290, and Los Alamos National Laboratory, Los Alamos, New Mexico 87545

Received December 9, 2003; E-mail: tjmeyer@lanl.gov

Abstract: Four new helical oligoproline assemblies containing 16, 17, 18, and 19 proline residues and ordered arrays of a Ru^{II}−bipyridyl chromophore and a phenothiazine electron-transfer donor have been synthesized in a modular fashion by solid-phase peptide synthesis. These arrays are illustrated and abbreviated as CH_3CO-Pro_6-Pra(PTZ)-Pro_n-Pra($Ru^{II}b_2m$)$^{2+}$-Pro_6-NH_2, where PTZ is 3-(10*H*-phenothiazine-10)propanoyl and ($Ru^{II}b'_2m$)$^{2+}$ is bis(4,4′-diethylamide-2,2′-bipyridine)(4-methyl,4′-carboxylate,2,2′-bipyridine)ruthenium(II) dication with $n = 2$ (**2**), 3 (**3**), 4 (**4**), and 5 (**5**). They contain PTZ as an electron-transfer donor and ($Ru^{II}b'_2m$)$^{2+}$ as a metal-to-ligand charge transfer (MLCT) light absorber and are separated by proline-to-proline through-space distances ranging from 0 ($n = 2$) to 12.9 Å ($n = 5$) relative to the $n = 2$ case. They exist in the proline-II helix form in water, as shown by circular dichroism measurements. Following laser flash $Ru^{II} \rightarrow b'_2m$ MLCT excitation at 460 nm in water, excited-state PTZ → Ru^{2+}* quenching (k_2) occurs by reductive electron transfer, followed by $Ru^+ \rightarrow PTZ^+$ back electron transfer (k_3), as shown by transient absorption and emission measurements in water at 25 °C. Quenching with $\Delta G° = -0.1$ eV is an activated process, while back electron transfer occurs in the inverted region, $\Delta G° = -1.8$ eV, and is activationless, as shown by temperature dependence measurements. Coincidentally, both reactions have comparable distance dependences, with k_2 varying from $= 1.9 \times 10^9$ ($n = 2$) to 2.2×10^6 s^{-1} ($n = 4$) and k_3 from $\sim 2.0 \times 10^9$ ($n = 2$) to 2.2×10^6 s^{-1} ($n = 4$). For both series there is a rate constant enhancement of ∼10 for $n = 5$ compared to $n = 4$ and a linear decrease in ln *k* with the through-space separation distance, pointing to a significant and probably dominant through-space component to intrahelical electron transfer.

Introduction

An important, continuing theme in electron-transfer chemistry is the study of long-range electron transfer through organic spacers.[1] Molecular assemblies based on oligoproline spacers have a special appeal because of the ease of synthesis of sequential oligomeric structures and the well-defined, relatively stable secondary structures that dominate when the oligoproline chain contains at least five consecutive proline residues.[2,3] Even with large appended substituents, the oligoproline array can still fold into a proline helix in solution.[4,5]

Previously, we reported light-induced electron-transfer quenching and back electron transfer in oligoproline arrays containing a combination of Ru^{II}−polypyridyl complexes and electron-transfer donors and acceptors.[4,6] Following $Ru^{II} \rightarrow$ polypyridyl metal-to-ligand charge-transfer (MLCT) excitation, rapid electron transfer occurs to give spatially separated oxidative and reductive equivalents. We report here the results of a study

§ Presently Associate Director for Strategic Research, MS A127, Los Alamos National Laboratory, P.O. Box 1663, Los Alamos, NM 87545.

(1) (a) Lang, K.; Kuki, A. *Photochem. Photobiol.* **1999**, *70*, 579−584. (b) Verhoeven, J. W. *Electron Transfer: From Isolated Molecules to Biomolecules*, Part 2; Jortner, J., Bixon, M., Eds.; John Wiley & Sons: New York, 1999; Vol. 107, pp 603−644. (c) Isied, S. S.; Ogawa, M. Y.; Wishart, J. F. *Chem. Rev.* **1992**, *92*, 381−394. (d) Ungar, L. W.; Newton, M. D.; Voth, G. A. *J. Phys. Chem. B* **1999**, *103*, 7367−7382. (e) Vassilian, A.; Wishart, J. F.; Hemelryck, B.; Schwarz, H.; Isied, S. S. *J. Am. Chem. Soc.* **1990**, *112*, 7278−7286. (f) Ogawa, M. Y.; Moreira, I.; Wishart, J. F.; Isied, S. S. *Chem. Phys.* **1993**, *176*, 589−600. (g) Ogawa, M. Y.; Wishart, J. F.; Young, Z.; Miller, J. R.; Isied, S. S. *J. Phys. Chem.* **1993**, *97*, 11456−11463. (h) Isied, S. S.; Vassilian, A. *J. Am. Chem. Soc.* **1984**, *106*, 1726−1732. (i) Fernando, S. R. L.; Kozlov, G. V.; Ogawa, M. Y. *Inorg. Chem.* **1998**, *37*, 1900−1905. (j) Isied, S. S.; Vassilian, A.; Magnuson, R. H.; Schwarz, H. A. *J. Am. Chem. Soc.* **1985**, *107*, 7432−7438. (k) Isied, S. S.; Moreira, I.; Ogawa, M. Y.; Vassilian, A.; Arbo, B.; Sun, J. *J. Photochem. Photobiol. A: Chem.* **1994**, *82*, 203−210. (l) Bobrowski, K.; Poznanski, J.; Holcman, J.; Wierzchowski, K. L. In *Photochemistry and Radiation Chemistry*: *Complementary Methods for the Study of Electron Transfer*; Wishart, J. F., Nocerq, D. G., Eds.; Advances in Chemistry Series 254; American Chemical Society: Washington, DC, 1998; pp 131−143. (m) Inai, Y.; Sisido, M.; Imanishi, Y. *J. Phys. Chem.* **1991**, *95*, 3847−3851. (n) Schanze, K. S.; Cabana, L. A. *J. Phys. Chem.* **1990**, *94*, 2740−2743.

(2) Deber, C. M.; Bovey, F. A.; Carver, J. P.; Blout, E. R. *J. Am. Chem. Soc.* **1970**, *92*, 6191.
(3) Okabayashi, H.; Isemura, T.; Sakakibara, S. *Biopolymers* **1968**, *6*, 323.
(4) McCafferty, D. G.; Friesen, D. A.; Danielson, E.; Wall, C. G.; Saderholm, M. J.; Erickson, B. W.; Meyer, T. J. *Proc. Natl. Acad. Sci. U.S.A.* **1996**, *98*, 8200−8204.
(5) McCafferty, D. G.; Friesen, D. A.; Slate, C. A.; Nakhle, B. M.; Graham, H. D.; Austell, T. L.; Vachet, R. W.; Mullis, B. H.; Erickson, B. W. *Tetrahedron* **1995**, *51*, 9859.
(6) Slate, C. A.; Striplin, D. R.; Moss, J. A.; Chen, P.; Erickson, B. W.; Meyer, T. J. *J. Am. Chem. Soc.* **1998**, *120*, 4885−4886.

10.1021/ja030659f CCC: $27.50

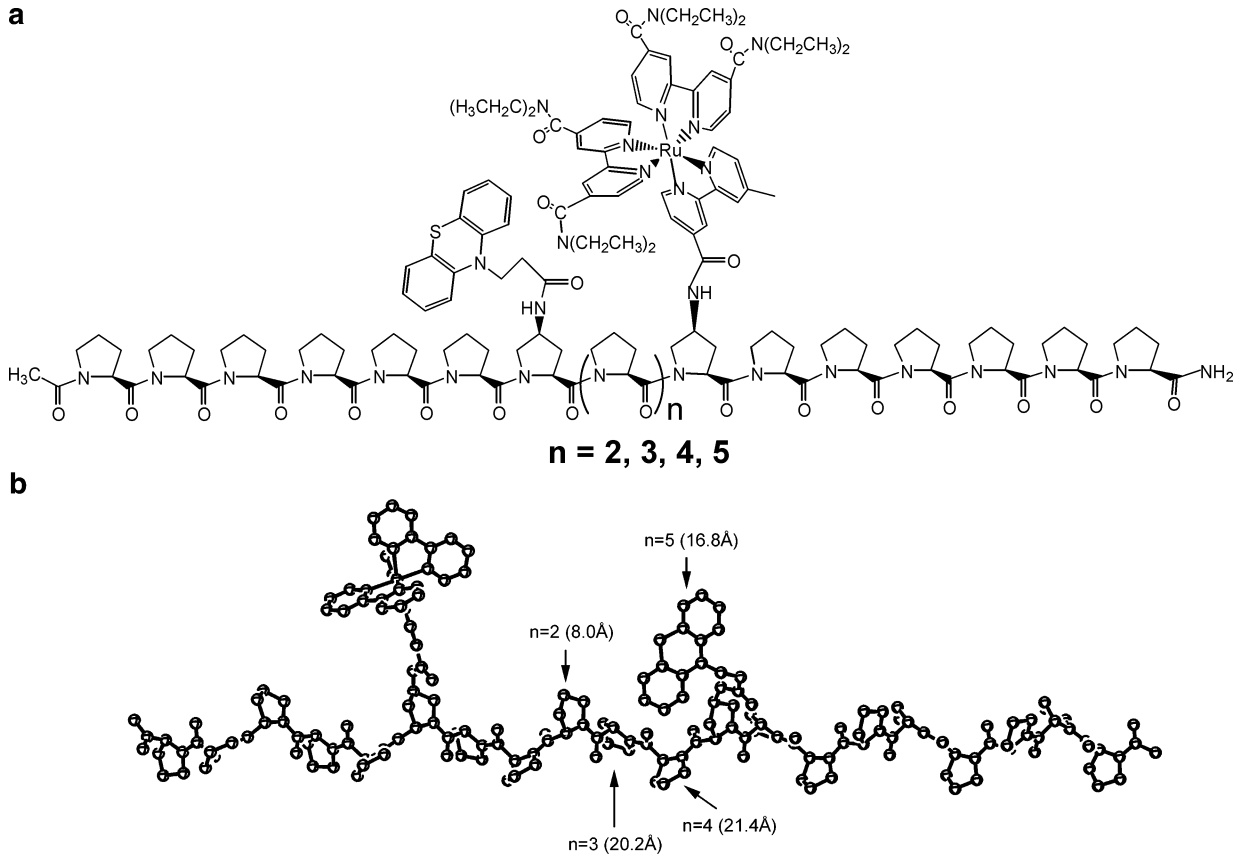

Figure 1. (a) Linear structures of oligoproline dyads **2**−**5**. (b) Energy-minimized, MM4-DFT computer-generated structure of the oligoproline dyads neglecting the $-C(O)NEt_2$ substituents on the bpy ligands. For clarity only array **5** is shown. The positions of PTZ in arrays **2**−**4** and the distance from the S-atom in PTZ to the ruthenium centers are denoted by the arrows. Computer-generated structures for **2**−**4** are included in the Supporting Information.

designed to explore the distance dependence of electron transfer for both excited-state quenching and back electron transfer in the series of oligoproline arrays, CH_3CO-Pro_6-Pra(PTZ)-Pro_n-Pra($Ru^{II}b'_2m$)$^{2+}$-Pro_6-NH_2, where PTZ is 3-(10*H*-phenothiazine-10)propanoyl[4] and ($Ru^{II}b'_2m$)$^{2+}$ = bis(4,4′-diethylamide-2,2′-bipyridine)(4-methyl-4′-carboxylate-2,2′-bipyridine)ruthenium(II) dication[8] with $n = 2$ (**2**), 3 (**3**), 4 (**4**), and 5 (**5**) (Figure 1a).

Experimental Section

Synthesis and Characterization. The redox sites in arrays **2**−**5** are joined by amide bonds to the oligoproline backbone, which was assembled by the manual, stepwise solid-phase method from Boc-Pro, Boc-Pro-Pro, and two derivatives of *cis*-*N*^{a}-Boc-4-amino-L-proline (Boc-Pra), the PF_6^- salt of ruthenium complex **1**,[7] ($Ru^{II}b'_2m$)$^{2+}$, and the PTZ derivative Boc-Pra(PTZ). Once the desired assembly was prepared as the PF_6^- salt, it was cleaved from the methylbenzhydrylamine resin with bromotrimethylsilane, isolated by HPLC on C_{18} butylsilica, and shown to be pure by analytical HPLC[8] and from the expected masses of 2904 (**2**), 3000 (**3**), 3096 (**4**), and 3194 Da (**5**) by electrospray ionization mass spectroscopy (Supporting Information Figure 1).

In water, circular dichroism measurements in the $\pi-\pi^*$/n$-\pi^*$ region (250−190 nm) of arrays **2**−**5** exhibited an intense negative feature at 205−209 nm and a weak positive feature at 226−228 nm (Supporting Information Figure 2). This pattern is consistent with substantial folding into the proline-II helix, which is left-handed with *trans*-amide bonds.[9,10]

Detailed descriptions of the synthetic procedures and characterization by mass spectroscopy and circular dichroism measurements are available elsewhere.[8]

Molecular Modeling. To construct realistic molecular models at an affordable computational cost given the size of the assemblies, we combined two theoretical methods manually. Starting from the crystal structure of polyproline,[11] we used the MM4 method as implemented in the package SPARTAN 5.11 (Wavefunction Inc.) to relax the polyproline backbone containing 20 proline units without any substituents. Since the orientation and geometry of the Ru(bpy) and PTZ units are crucial for the spatial distances, we employed high-level ab initio methods based on density functional theory (DFT) to determine the structure of a Ru(bpy)−proline monomer. The Amsterdam Density Functional (ADF 1999) package[12] was used to fully optimize the structures of nonsubstituted Ru(bpy)-proline and PTZ-proline fragments. A triple-ζ STO basis set containing one set of polarization functions as provided with the package (Basis IV, comparable to 6-311G*) was used with a VWN local exchange-correlation potential, augumented by exchange and correlation functionals as suggested by Perdew and Wang (PW91).[13] The inner core shells were treated by application of the frozen-core approximation. By using the bond lengths and angles

(7) Serron, S. A.; Aldridge, W. S.; Danell, R. M.; Meyer, T. J. *Tetrahedron Lett.* **2000**, *41*, 4039−4042.
(8) Aldridge, S. A. Ph.D. Thesis, University of North Carolina, Chapel Hill, NC, 2000.
(9) Woody, R. W. *Conformation in Biology and Drug Design*; Academic Press: NewYork, 1985; Vol. 7.
(10) Slate, C. A.; Binstead, R. A.; Meyer, T. J.; Erickson, B. W. *Lett. Pept. Sci.* **1999**, *6*, 61−69.
(11) (a) Traub, W.; Shmueli, U. *Nature* **1963**, *198*, 1165. (b) Cowan, P. M.; McGavin, S. *Nature* **1955**, *176*, 501.
(12) (a) *ADF 1999*; Vrije Universiteit Amsterdam: Amsterdam, The Netherlands, 1999. (b) Baerends, E. J.; Ellis, D. E.; Ros, P. *Chem. Phys.* **1973**, *2*, 41. (c) te Velde, G.; Baerends, E. J. *J. Comput. Phys.* **1992**, *99*, 84. (d) Fonseca Guerra, C.; et al. *METECC-95* **1995**, 305.
(13) (a) Vosko, S. H.; Wilk, L.; Nusair, M. *Can. J. Phys.* **1980**, *58*, 1200. (b) Perdew, J. P.; Wang, Y. *Phys. Rev. B* **1992**, *45*, 13244.

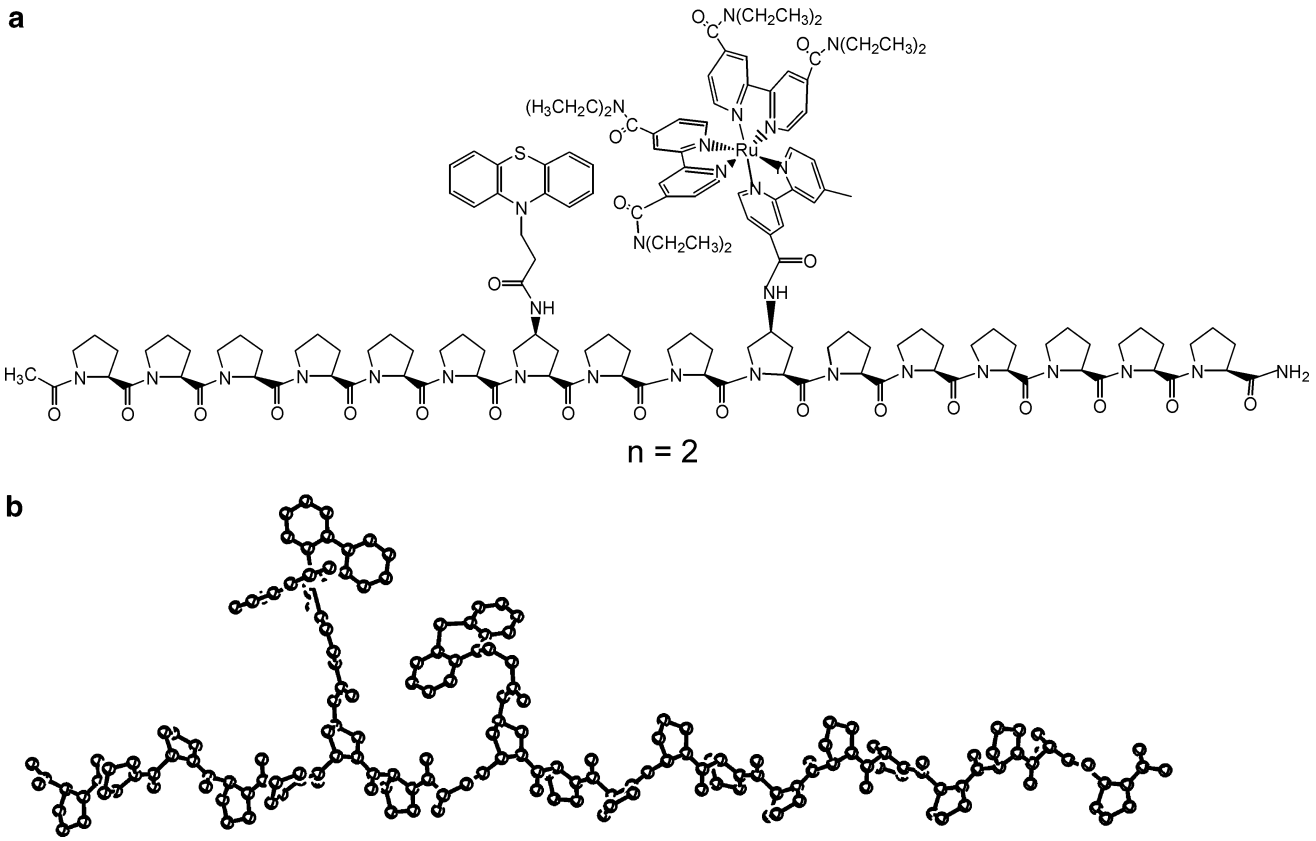

Figure 2. As in Figure 1, illustrating (a) the linear structure of array **2** and (b) the computer-generated structure.

found in these high-level calculations, we manually constructed a substituted polyproline chain.

Measurements. Emission lifetime measurements on the >20 ns time scale were recorded by using a PRA LN1000 nitrogen laser (337 nm) as a pulsed source (3 Hz) to pump a PRA LN102/1000 tunable dye laser with coumarin 460. The sub-nanosecond measurements on **2** were made by time-correlated single-photon counting on an apparatus that has been described in detail elsewhere.[14] Quantum yield measurements were made in argon-deaerated solutions relative to $[Ru(bpy)_3]^{2+}$*.

Transient absorption difference spectra and decays were measured in argon-deaerated water following Nd:YAG laser flash excitation at 460 nm, 5.9 mJ/pulse (3.8 cm^2). Difference spectra and decay kinetics were acquired, following excitation at a variety of wavelengths from 380 to 520 nm.[15]

Electrochemical measurements were conducted in argon-deaerated acetonitrile with tetra-*n*-butylammonium hexafluorophosphate as the supporting electrolyte with a Pt working electrode, $Ag/AgNO_3$ reference electrode, and Pt wire as the counter electrode with 100 mV/s current sweeps. Because of the higher dielectric constant, $\Delta G°$ should be slightly more favorable in water for the quenching step, consistent with the quenching data. It was not possible to make measurements in water because of the irreversibility of the $-PTZ^{+/0}$ couple.

Results

Generic linear and energy-minimized computer-generated structures of the oligoproline arrays are shown in Figure 1, and both types of structures for array **2** are shown in Figure 2. As a simplification, the calculations were conducted on assemblies without the diethylamide substituents on the bpy ligands.

Arrays **2**−**5** have characteristic $Ru^{II} \rightarrow$ polypyridyl MLCT absorption bands in water centered at 464 nm. Emission from **1** occurs at 646 nm with emission quantum yield, $\Phi_{em} = 0.047 \pm 0.009$ and lifetime, $\tau = 520$ ns with 640 nm monitoring in deaerated water.

Photochemical electron transfer in **2**−**5** was investigated by laser flash photolysis with emission monitoring for excited-state quenching and absorption monitoring for both quenching and back electron transfer. Compared to **1**, emission from **2** ($\Phi_{em} = 0.0030 \pm 0.0009$, $\tau = 53 \pm 11$ ns) is 94% quenched, **3** ($\Phi_{em} = 0.0059 \pm 0.0012$, $\tau = 56 \pm 11$ ns) is 87% quenched, **4** ($\Phi_{em} = 0.016 \pm 0.003$, $\tau = 170 \pm 34$ ns) is 66% quenched, and **5** ($\Phi_{em} = 0.0058 \pm 0.0012$, $\tau = 41 \pm 8$ ns) is 88% quenched.

A small component of unquenched emission was observed from arrays **2**−**5** with $\tau = 1000$ ns. This is common in PTZ-containing arrays and is probably due to partial oxidation of PTZ to the *S*-oxide during workup.[4] In acetonitrile, electron-transfer quenching was less efficient, with 92% quenching observed for **2**, 30% for **3**, 47% for **4**, and 24% for **5** at room temperature.

Luminescence decays for arrays **3**−**5** were fit to the biexponential function, $I(t) = I_1 \exp(-k_1 t) + I_2 \exp(-k_2 t)$. The longer lifetime in the fits corresponds to that of the model and is due to the small amounts of unquenched impurities mentioned above. The kinetics for array **2** were more complex but could be adequately represented by a sum of three exponentials. In all cases, luminescence was monitored at 640 nm following 460 nm excitation.

The results of the transient absorption measurements were consistent with the sequence of reactions in eq 1 in the appearance of transient features for PTZ^+ at 520 nm and the

(14) Fleming, C. N.; Maxwell, K. A.; Papanikolas, J. M.; Meyer, T. J. *J. Am. Chem. Soc*. **2001**, *123*, 10336.
(15) Transient absorption measurements were performed using an apparatus described previously: Maxwell, K. A.; Sykora, M.; DeSimone, J. M.; Meyer, T. J. *Inorg. Chem.* **2000**, *39*, 71−75.

Table 1. Kinetic and Structural Parameters for Forward and Reverse Electron Transfer in the Oligoprolines in Water at 25 °C

array	d (Å)[a]	no. of proline spacers[b]	$r - r_0$ (Å)[c]	$d - d_0$ (Å)[d]	k_2 (s^{-1})[e] ($k_2'(d_0)$, s^{-1})[f]	k_3 (s^{-1})[e] ($k_3'(d_0)$, s^{-1})[f]
2	8.0 (5.0)	2	0	0	1.9×10^9	$\sim 2.0 \times 10^9$
3	20.2 (17.2)	3	4.3 (3.1)	12.2	1.8×10^7 (3.1×10^7)	2.3×10^7 (1.6×10^7)
4	16.8 (13.8)	4	8.6 (6.2)	13.4	2.2×10^6 (3.8×10^6)	2.2×10^6 (1.5×10^6)
5	21.4 (18.4)	5	12.9 (9.3)	8.8	2.4×10^7 (3.8×10^7)	1.5×10^7 (1.1×10^7)

[a] Through-space separation distance between the sulfur of PTZ and the center of the ruthenium complex in the energy-minimized structures. Values in parentheses are through-space distances for back electron transfer from the center of the nearest bpy ligand to the sulfur of the PTZ. [b] Number of proline spacers between the chromophore and PTZ-bearing prolines. [c] Through-bond separation distance through the proline spacer relative to $n = 2$. The $r - r_0$ values are the calculated through-bond distances, and the values in parentheses through-ring distances; see text. [d] Through-space separation distance relative to $n = 2$. [e] Uncertainties are ±10%. [f] k_2 corrected for the distance dependence of λ_o by using eq 11 to calculate k_2 if $d - d_0$ was 0. Similarly for k_3 by using eq 15; see text.

reduced complex at 380 nm. Back electron transfer was monitored at the PTZ^+ absorption maximum at 520 nm following 460 nm excitation and followed exponential kinetics.

From known redox potentials, $E_{1/2} = 1.41$ V (vs SSCE) for the $Ru^{III/II}$ couple of complex **1**, $\Delta G° = -0.1$ eV for the quenching step, k_2 in eq 1, and $\Delta G° = -1.8$ eV for back electron transfer in k_3.[4]

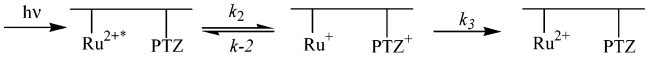

(1)

Rate constants obtained from the kinetic fits are listed in Table 1. The temperature dependences of the rate constants for both forward (k_2) and back electron transfer (k_3) were investigated in water over the temperature range 2−37 °C for array **3**. The data were fit to the reaction rate theory expression in eq 2. In

$$\ln\frac{k}{T} = \ln\frac{k_B}{h} - \frac{\Delta H^‡}{RT} + \frac{\Delta S^‡}{R} \qquad (2)$$

eq 2, k_B is the Boltzmann constant, T the absolute temperature, h Planck's constant, R the gas constant, $\Delta H^‡$ the enthalpy of activation, and $\Delta S^‡$ the entropy of activation. From a plot of ln k/T vs $1/T$, for the quenching step for array **3** (k_2 in eq 1), $\Delta H^‡ = 1.7 \pm 0.1$ kcal/mol^{-1} and $\Delta S^‡ = -3 \pm 3$ eu from transient absorbance measurements and $\Delta H^‡ = 1.5 \pm 0.1$ kcal/mol^{-1} and $\Delta S^‡ = -6 \pm 3$ eu from the emission measurements. Back electron transfer (k_3 in eq 1), which occurs in the inverted region, was activationless with $\Delta H^‡ \approx 0$ and $\Delta S^‡ \approx -20$ eu.

Discussion

The kinetics data in Table **1** show that both quenching and back electron transfer vary significantly with the number of proline spacers and, by inference, the distance between electron donors and acceptors. The calculated structures of arrays **2** and **5**, but with 2,2′-bipyridine rather than 4,4′-diethylamide-2,2′-bipyridine to simplify the calculations, are shown in Figures 1 and 2. The structures were calculated by a combination of molecular mechanics (MM4) and density functional theory (DFT) as described in the Experimental Section.

The positions of PTZ attachment in arrays **2**−**4**, which are also indicated in Figure 1, are the center-to-center, through-space distances. In these calculations, through-space separation distances for quenching were taken as the center-to-center distances between the S atom of PTZ and the center of the complex. For back electron transfer, the distance was calculated from the S-atom to a point 3.0 Å from the Ru center at the center of the nearest b′ ligand.[16,17] In these structures, the tilt of the PTZ toward the amide group of the proline linker is due to a strong H-bonding interaction (~3 kcal/mol) with the amide N−H bond, as revealed by the structure calculations. By utilizing slightly higher energy rotameric structures and recognizing the possible spatial influence of the diethylamide substituents in delocalizing the electronic wave functions, the actual through-space distance could be slightly less than the calculated values cited in Table 1.

Quenching. Electron Transfer in the Normal Region. The rate constant for electron transfer, k_{ET}, is given in eq 3. It

$$k_{ET} = \frac{2\pi H_{DA}^2}{\hbar}\sum_{\nu'} \exp - (S)\frac{S^{\nu'}}{\nu'!}\exp\left[\frac{(\lambda_{o,L} + \Delta G° + \nu'\eta\omega)^2}{4\lambda_{o,L}RT}\right] \qquad (3)$$

assumes the average mode approximation for a single high- or medium-frequency coupled vibration of quantum spacing $\hbar\omega$ and product quantum number ν' with $\hbar\omega = h\nu \gg k_BT$.[18−21] It also assumes the same quantum spacing before and after electron transfer with $\hbar\omega = \hbar\omega'$. In eq 3, H_{DA} is the electron-transfer matrix element, S the electron−vibrational coupling constant, and $\lambda_{o,L}$ the solvent reorganizational energy, including a contribution from low-frequency intramolecular vibrations treated classically, $\lambda_{i,L}$. $\lambda_{o,L} = \lambda_{i,L} + \lambda_o$ with λ_o the solvent reorganization energy. k_{ET} is the sum of transitions through vibrational channels from the $\nu = 0$ level initially to levels ν' in the product. S is related to the change in equilibrium displacement for the coupled mode, ΔQ_{eq}, by

$$S = \frac{1}{2}\left(\frac{M\omega}{\hbar}\right)(\Delta Q_{eq})^2 \qquad (4)$$

where M is the reduced mass.[18−21]

For the quenching and back electron-transfer steps in eq 1, it is known that a series of ring-stretching modes on bpy and PTZ

(16) Kober, E. M.; Sullivan, B. P.; Meyer, T. J. *Inorg. Chem.* **1984**, *23*, 2098−2104.
(17) Smith, G. D.; Maxwell, K. A.; DeSimone, J. M.; Meyer, T. J.; Palmer, R. A. *Inorg. Chem.* **2000**, *39*, 893−898.
(18) (a) Marcus, R. A. *Annu. Rev. Phys. Chem.* **1966**, *15*, 155. (b) R. A. Marcus Commemorative Issue, *J. Phys. Chem.* **1986**, *90*. (c) Huang, K.; Rhys, A. *Proc. R. Soc.* **1950**, *A204*, 406.
(19) Kestner, N. R.; Logan, J.; Jortner, J. *J. Phys. Chem.* **1974**, *78*, 2148.
(20) Jortner, J. *J. Chem. Phys.* **1976**, *64*, 4860.
(21) Chen, P.; Meyer, T. J. *Chem. Rev.* **1998**, *98*, 1439.

are coupled to electron transfer.[4] From this analysis, $\hbar\omega \approx 1300$ cm^{-1} in eq 3. If it is assumed that participation by these modes is dominated by $\upsilon = 0 \rightarrow \upsilon' = 0$ vibrational tunneling, k_{ET} for the quenching step (k_2) is given by

$$k_{ET} = k_2 \approx \frac{2\pi {H_{DA}}^2}{\hbar} \exp(-S) \exp -\left[\frac{(\lambda_{o,L} + \Delta G^\circ)^2}{4\lambda_{o,L}RT}\right] \quad (5)$$

For the quenching reaction, $\Delta G^\circ \approx 0.1$ eV, $|\Delta G^\circ|^2 \ll 4\lambda$, and eq 5 becomes

$$k_{ET} = k_2 \approx \frac{2\pi {H_{DA}}^2}{\hbar} \exp(-S) \exp\left(\frac{-\Delta G^\circ}{2RT}\right) \exp\left(\frac{-\lambda_{o,L}}{4RT}\right) \quad (6a)$$

The solvent-dependent part of $\lambda_{o,L}$ is λ_o. Separating $\lambda_{i,L}$ and λ_o gives

$$k_{ET} = k_2 \approx \frac{2\pi {H_{DA}}^2}{\hbar} \exp(-S) \exp\left(-\frac{(2\Delta G^\circ + \lambda_{i,L})}{4RT}\right) \exp\left(\frac{-\lambda_o}{4RT}\right) \quad (6b)$$

Based on eq 6, there are two potential contributors to the distance dependence of k_{ET}. They are the extent of electronic coupling and its influence on the electron-transfer matrix element, H_{DA}. The second arises from the distance dependence of the solvent reorganizational energy.[21−23] There is also a distance dependence arising from a work term correction in converting the electrochemical data into ΔG°, but it is negligible in water due to its high static dielectric constant, $D_s = 78$.[21,24]

Assuming two non-interpenetrating spheres, the distance dependence of λ_o is given by eq 7, in which a_1 and a_2 are the radii of the redox sites, D_{op} and D_s are the optical and static dielectric constants of the solvent, and d is the center-to-center separation distance.

$$\lambda_o = \frac{e^2}{4}\left(\frac{1}{2a_1} + \frac{1}{2a_2} - \frac{1}{d}\right)\left(\frac{1}{D_{op}} - \frac{1}{D_s}\right) \quad (7)$$

In accounting for the distance dependence of λ_o and its influence on k_{ET}, it is useful to factor it into the sum of $\lambda_o(d_0)$, which is λ_o at the reference distance of 8.0 Å for the $n = 2$ oligoproline array, and $\lambda_o(d - d_0)$, the distance dependence of λ_o past $d - d_0$,

$$\lambda_o = \lambda_o(d_0) + \lambda_o(d - d_0) \quad (8a)$$

The latter is given by

$$\lambda_o(d - d_0) = e^2\left(\frac{1}{d_0} - \frac{1}{d}\right)\left(\frac{1}{D_{op}} - \frac{1}{D_s}\right) \quad (8b)$$

The distance dependence of k_{ET} from this source is given by

$$k_{ET}(d) = k_2(d) = k_2(d_0) \exp -\left[\frac{e^2}{4RT}\left(\frac{1}{d_0} - \frac{1}{d}\right)\left(\frac{1}{D_{op}} - \frac{1}{D_s}\right)\right] \quad \text{(normal region)} \quad (9)$$

k_{ET} (d_0) is the rate constant at separation distance 8.0 Å for $n = 2$.

An additional distance dependence is introduced into k_{ET} through H_{DA}, which falls off exponentially with distance. If a single, through-bond orbital pathway is assumed, and the distance dependence of λ_o is neglected, k_{ET} is predicted to vary with r as shown in eq 10.[1] In eq 10, β is the distance attenuation factor in Å^{-1} and $k_{ET}(r_o)$ is the rate constant at r_o.

In calculating average through-bond distances in earlier studies, r_o was estimated as the sum of the total number of prolines in an assembly, with the proline length taken as 3.1 Å based on its crystal structure.[25] The shortest through-bond distance through a single proline unit on a bond-for-bond basis and from literature values for the individual bond lengths is 4.3 Å.[26]

$$k_{ET} = k_{ET}(r) = k_{ET}(r_o) \exp -[\beta(r - r_0)] \quad (10)$$

If H_{DA} is dominated by a single through-space pathway, rather than by a through-bond pathway or pathways, k_{ET} is predicted to vary with d as shown in eq 10a. Again, this equation neglects

$$k_{ET} = k_{ET}(d) = k_{ET}(d_o) \exp -[\beta(d - d_0)] \quad (10a)$$

the distance dependence of λ_o. There is potential ambiguity in the through-space distances as well. The distances used in the correlations were based on the structures shown in Figures 1 and 2, which include a strong (~3 kcal/mol) NH···O═C H-bond interaction, leading to the tilt of the PTZ donor. In water, there is competitive H-bonding with the solvent, which may decrease the relative stability of the H-bonded structure. Even so, through-space electron transfer will be dominated by rotameric configurations which minimize the through-space distances, and those distances are closely approximated by the H-bonded distances.

In applying eq 3 to the series $n = 2-5$, it is convenient to take $r_0 = 0$ for the through-bond separation distance from proline to proline with no proline spacers. With this definition, only rate constant variations due to the increase in the number of proline spacers are taken into account. The electron-transfer donors and acceptors, their proline connectors, and the associated electronic wave functions remain constant in the series.

Through-bond or through-space orbital pathways or a combination of the two may play important roles throughout the $n = 2-5$ series. To isolate the distance dependence of k_{ET} arising solely from electronic effects, it is necessary to correct the experimental $k_{ET} = k_2$ values for the distance dependence of the solvent reorganization energy. The experimental rate constant can then be corrected to what it would be at d_0. One way of doing this is to reference the solvent reorganization energies to the value at the fixed through-space distance d_0 by defining the quantity $k'(d_0)$ as

$$k'(d_0) = k_2 \exp\left[\frac{e^2}{4RT}\left(\frac{1}{d_0} - \frac{1}{d}\right)\left(\frac{1}{D_{op}} - \frac{1}{D_s}\right)\right] \quad \text{(normal region)} \quad (11)$$

According to eq 10, for through-bond electron transfer, $k_2'(r,d_0)$

(22) Marcus, R. A.; Sutin, N. *Comm. Inorg. Chem.* **1986**, *5*, 115.
(23) Sutin, N. *Advances in Chemical Physics, Electron Transfer—From Isolated Molecules to Biomolecules*, Part 1; Jortner, J., Bixon, M., Eds.; John Wiley & Sons: New York, 1999; Vol. 109, pp 7−33.
(24) Mecklenburg, S. L.; Peek, B. M.; Schoonover, J. R.; McCafferty, D. G.; Wall, C. G.; Erickson, B. W.; Meyer, T. J. *J. Am. Chem. Soc.* **1993**, *115*, 5479.
(25) Cowan, P. M.; McGavin, S. *Nature* **1955**, *176*, 501.
(26) Bowen, H. J. M.; Sutton, L. In *Tables of interatomic distances and configuration in molecules and ions*; Sutton, L. E., Jenkin, D. G., Mitchell, A. D., Cross, L. C., Eds.; Chemical Society: London, 1958.

should vary with $r - r_0$ as

$$k_2'(r,d_0) = k_2(r_0,d_0) \exp - [\beta_2(r - r_0)] \qquad (12)$$

β_2 is the distance attenuation factor for electron transfer in the quenching reaction. Values of $k_2'(r,d_0)$ calculated from the experimental k_2 values and the calculated values for d_0 and d are listed in Table 1.

Back Electron Transfer in the Inverted Region. Back electron transfer is highly favored ($\Delta G° = -1.8$ eV) and occurs in the inverted region where $|\Delta G°| > \lambda$ and λ is the total reorganization energy. This is also a characteristic of excited-state nonradiative decay, but the two are fundamentally different processes.[21,28,29] Electron transfer in the inverted region involves a "redox-separated" (RS) state where, in contrast to an excited state, electronic coupling between the electron donor and acceptor is weak. In the limits $|\Delta G°| \gg S\hbar\omega$ and $\hbar\omega \gg k_BT$, the sum over vibrational levels expression in eq 3 is accurately represented by the energy gap law result in eq 13.[20,21,28]

$$k_{ET} = \frac{2\pi H_{DA}^{\,2}}{\hbar}\left(\frac{1}{\hbar\omega E_0}\right)^{1/2} \exp -(S) \exp -\frac{\gamma E_0}{S\hbar\omega} \exp\left(\frac{\gamma + 1}{\hbar\omega}\right)^2 \lambda_{o,L} RT \qquad (13)$$

$$\gamma = \ln\left(\frac{E_0}{S\hbar\omega}\right) - 1 \qquad (13a)$$

In this expression, E_0 is the $v' = 0 \rightarrow v = 0$ emission energy gap, which is related to $\Delta G°$ by

$$|\Delta G°| = E_0 + \lambda_{o,L} \qquad (13b)$$

Based on eq 13, the distance dependence for k_{ET} in the inverted region arising from the solvent is given by

$$k_{ET}(d) = k_3(d) = k_3(d_0) \exp\left(\frac{\gamma + 1}{\hbar\omega}\right)^2 \lambda_o(d - d_0)RT \qquad (14a)$$

with

$$k_3(d_0) = \frac{2\pi H_{DA}^{\,2}}{\hbar\omega}\left(\frac{1}{\hbar\omega E_0}\right)^{1/2} \exp(-S) \exp\left(-\frac{\gamma E_0}{S\hbar\omega}\right) \qquad (14b)$$

and $\lambda_o(d - d_0)$ defined in eq 8. The quantity $[(\gamma + 1)/\hbar\omega]^2 e^2 RT(1/2a_1 + 1/2a_2 - 1/d) = 1.2$ was evaluated experimentally in an earlier solvent dependence study on back electron transfer in $[Re^I(4\text{-Mebpy}^{\bullet-}\text{-}4'\text{-}CH_2PTZ^{\bullet+})(CO)_3(Cl)]$.[27] On the basis of this value, it is possible to correct the $k_{ET} = k_3$ values for differences in solvent reorganization energy to the common distance d_0 by defining the quantity $k_3'(d_0)$ as in eq 15.

$$k_3'(d_0) = k_3 \exp -5.0\left[\left(\frac{1}{d_0} - \frac{1}{d}\right)\left(\frac{1}{D_{op}} - \frac{1}{D_s}\right)\right] \quad \text{(inverted region)} \qquad (15)$$

For through-bond electron transfer,

$$k_3'(r,d_0) = k_3(r_0,d_0) \exp -[\beta_3(r - r_0)] \qquad (16a)$$

with β_3 the attenuation factor for back electron transfer. For through-space electron transfer,

$$k_3'(d,d_0) = k_3(d_0) \exp -[\beta_3(d - d_0)] \qquad (16b)$$

Rate constants corrected for the solvent distance dependence of k_{ET} in the inverted region are also listed in Table 1. As a reminder, the through-space distances in this case are less than those for the quenching step because electron transfer occurs from a π^* orbital centered on the 4,4′-$(CONEt_2)$bpy ligand.

Distance Dependence of Electron Transfer. As noted above, the electron-transfer rate constant acquires a distance dependence from two sources, coupling with the surrounding medium, which varies with the internuclear separation distance d, and electronic coupling, which varies with distance r for through-bond electron transfer or d for through-space electron transfer. When expressed relative to a reference geometry at $r = r_0$, $d = d_0$, k_{ET} varies with r and d for through-bond electron transfer as

$$k_{ET} = k_{ET}(r,d) = k_{ET}(r_0,d_0) \exp -[\beta(r - r_0)] \times \exp \delta\left[e^2\left(\frac{1}{d_0} - \frac{1}{d}\right)\left(\frac{1}{D_{op}} - \frac{1}{D_s}\right)\right] \qquad (17)$$

with

$$\delta = -\frac{1}{4RT} \qquad \text{(normal electron transfer)} \qquad (18a)$$

$$\delta = \left(\frac{\gamma + 1}{\eta\omega}\right)^2 RT \qquad \text{(inverted electron transfer)} \qquad (18b)$$

The equivalent expression for through-space electron transfer is

$$k_{ET} = k_{ET}(d) = k_{ET}(d_0) \exp -[\beta(d - d_0)] \times \exp \delta\left[e^2\left(\frac{1}{d_0} - \frac{1}{d}\right)\left(\frac{1}{D_{op}} - \frac{1}{D_s}\right)\right] \qquad (19)$$

The distance dependence in λ_o arises from the changes in solvent polarization that accompany site-to-site electron transfer and depends on the through-space geometrical separation distances. That distance is longer for electron-transfer quenching in the oligoproline arrays because electron transfer occurs from the appended PTZ to a dπ orbital centered on Ru. The change in sign for the quantity δ between normal and inverted electron transfer is a consequence of a fundamental difference in the microscopic mechanisms.[21] In the normal region, the solvent reorganization energy adds to the classical barrier, which increases as d increases. In the inverted region, the excess energy released on electron transfer appears in the coupled intramolecular and collective solvent modes. This is enhanced by stronger coupling with the solvent.

Comparisons of the kinetic data in Table 1 for the oligoproline arrays provide a useful experimental probe of distance effects. The only change in molecular structure between oligomers is in the number of proline spacers between the electron-transfer donor and acceptor.

The ability to study electron transfer in both directions, one in the normal and one in the inverted region, is a novel feature

(27) Chen, P.; Mecklenburg, S. L.; Duesing, R.; Meyer, T. J. *J. Phys. Chem.* **1993**, *97*, 13126.
(28) Kober, E. M.; Caspar, J. V.; Lumpkin, R. S.; Meyer, T. J. *J. Phys. Chem.* **1986**, *90*, 3722.
(29) Claude, J. P.; Omberg, K. M.; Williams, D. S.; Meyer, T. J. *J. Phys. Chem. A* **2002**, *106*, 7795.

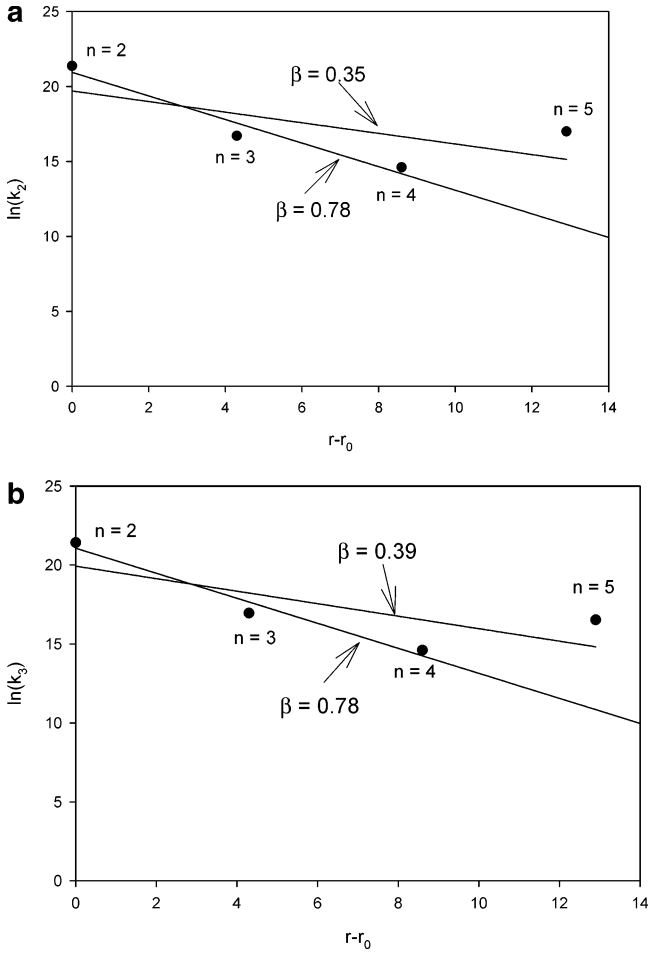

Figure 3. (a) Plots of ln k_{ET} vs $r - r_o$ for electron-transfer quenching (normal region). (b) As in panel a for back electron transfer (inverted region). For the fits to all four experimental points, $\beta = 0.35$ Å^{-1}, $k_2(r_0,d_0) = 3.5 \times 10^8$ s^{-1} for panel a and $\beta = 0.39$ Å^{-1}, $k_2(r_0,d_0) = 4.5 \times 10^8$ s^{-1} for panel b.

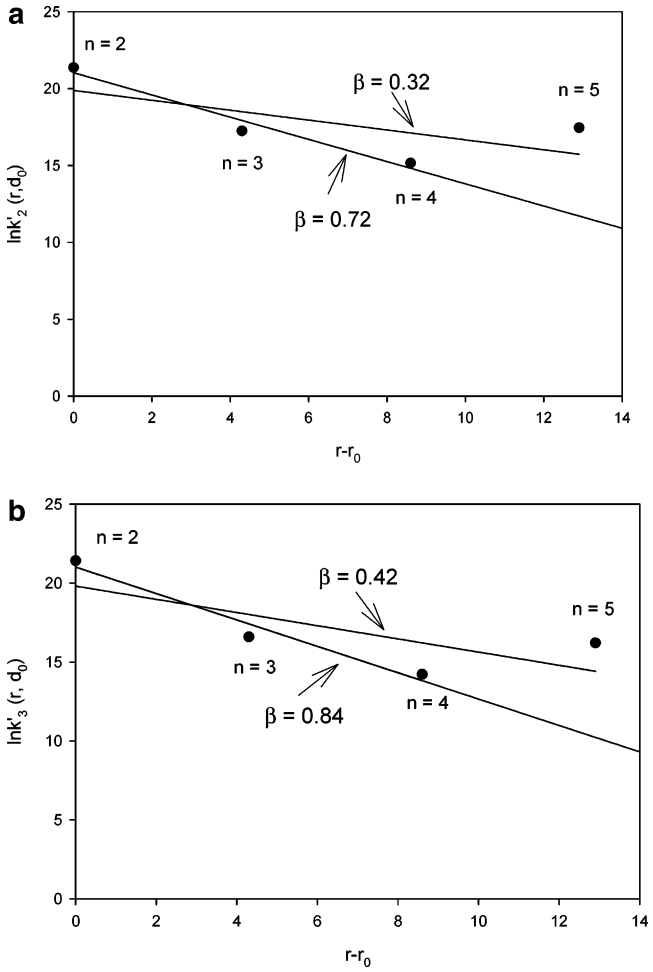

Figure 4. As in Figure 3, with the rate constants in Figure 3 normalized for the predicted distance dependence of the solvent reorganization energy, plotted vs $r - r_0$ for (a) quenching ($\beta = 0.32$ Å^{-1}, $k_2'(r_0,d_0) = 4.3 \times 10^8$ s^{-1}, normal region) and (b) back electron transfer ($\beta = 0.42$ Å^{-1}, $k_3'(r_0,d_0) = 4.0 \times 10^8$ s^{-1}, inverted region).

of the oligoprolines used here. The fact that the rate constants for quenching and reverse electron transfer are nearly the same is a coincidence and only true near 25 °C. As shown by the temperature dependence studies on array **3**, the reactions have significantly different activation parameters. The reverse reaction occurs deeply in the inverted region, is dominated by vibrational overlap of ν(bpy) modes between reactant and product states, and, as expected, is activationless. The quenching step occurs in the normal region and includes a significant contribution from thermally activated classical barrier crossing.

To explore the distance dependence of k_{ET} that arises from electronic coupling requires that the experimental data be corrected for the distance dependence of λ_o. The approach that we took was to normalize the solvent contribution to the electron-transfer barrier to a common through-space distance, d_0, by using eqs 11 and 15. This led to the $k_2'(d_0)$ and $k_3'(d_0)$ listings in Table 1.

Plots of ln(k_{ET}) with k_{ET} uncorrected for the solvent distance dependence are shown for $n = 2-5$ in Figure 3, and plots of ln(k_{ET}) with the solvent correction are shown shown in Figure 4. In both plots, the shortest through-bond distance through an individual proline spacer was taken to be 4.9 Å. A plot with this distance taken as 3.1 Å is shown in Supporting Information Figure 3a.

With only four experimental points, it is not possible to obtain statistically significant correlations to the distance-dependent data. The linear correlations in Figures 3−5 are only suggestive, but are of value in making comparisons with the results of earlier studies. From the best-fit straight line through only the points for $n = 2-4$, in Figure 3a, $\beta = 0.78$ Å^{-1} and $k_{ET}(r_0) = k_2(r_0) = 1.2 \times 10^9$ s^{-1}. With the solvent correction, $\beta = 0.72$ cm^{-1} and $k_2(r_0) = 1.4 \times 10^9$ s^{-1}. By using the shorter proline spacer distances and no solvent correction, $\beta = 1.1$ Å^{-1} and $k_2(r_0) = 1.2 \times 10^9$ s^{-1}.

The values $\beta = 0.78$ and 1.1 Å^{-1} can be compared to β values obtained from distance dependence studies based on proline spacers at short separation distances by Isied and co-workers ($n = 0-3$; $\beta = 0.65$ Å^{-1})[1j] and in the quenching of a Re^{II}-(bpy$^{\bullet-}$)-based MLCT excited state by an appended aromatic amine ($\beta = 1.0$ Å^{-1}).[1n]

If all four points in Figure 3a are included without the solvent correction, the correlation is essentially lost, but a best-fit straight line gives $\beta = 0.35$ Å^{-1} and $k_2(r_0,d_0) = 3.5 \times 10^8$ s^{-1}. This β value is comparable to values obtained by Isied and co-workers for longer separation distances ($n = 4-6$; $\beta \approx 0.3$ Å^{-1}) in their studies based on oligoproline spacers.[1g]

From the data in Figure 3b, a related observation is made in the dependence of ln(k_3) on $r - r_0$ in the inverted region. In

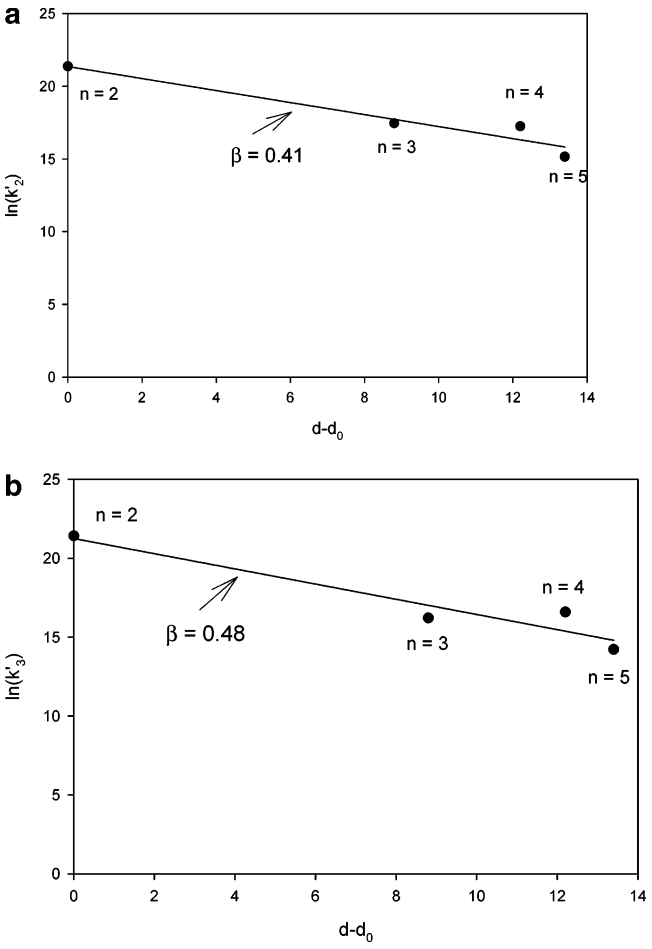

Figure 5. As in Figure 3, with the rate constants in Figure 3 normalized for the distance dependence of λ_o, plotted vs $d - d_0$ for (a) quenching ($\beta = 0.41$ Å^{-1}, $k_2'(d_0) = 1.9 \times 10^9$ s^{-1}) and (b) back electron transfer ($\beta = 0.48$ Å^{-1}, $k_3'(d_0) = 1.7 \times 10^9$ s^{-1}) in the inverted region.

this case, the best straight line through the points with $n = 2-4$ has $\beta = 0.78$ Å^{-1} and $k_3(r_0,d_0) = 1.4 \times 10^9$ s^{-1}, and with the solvent correction included, $\beta = 0.84$ Å^{-1} and $k_3'(r_0,d_0) = 1.3 \times 10^9$ s^{-1}. For the correlations involving all four points, $\beta = 0.39$ Å^{-1} and $k_3'(r_0,d_0) = 4.5 \times 10^8$ s^{-1} for the data in Figure 3b and $\beta = 0.42$ Å^{-1} and $k_3'(r_0,d_0) = 4.0 \times 10^8$ s^{-1} for the solvent-corrected data.

It could be argued that there is evidence in the kinetics data for more than one pathway by the significant increase in k_{ET} for **5** compared to **3** or **4** for both quenching and back electron transfer. In this series, the through-space distances for **5** (16.8 and 13.8 Å) are significantly less than for **3** (20.2 and 12.2 Å) or **4** (21.4 and 18.4 Å) because of the repeat structure of the helix, Figure 1b.

Sisido and co-workers have made a similar observation in the quenching of pyrene fluorescence by an appended dimethylaniline derivative in α-helices of polyalanine[1m] and attributed it to through-space electron transfer.

Mechanism of Electron Transfer: Through-Space or Through-Bond? As can be seen by comparing the experimental (k_2,k_3) and solvent-normalized (k_2',k_3') rate constants in Table 1, the point-by-point solvent corrections are significant. They vary in opposite directions with distance ($d - d_0$), with the correction varying from ~30% to ~ 70%. As shown by the plots of $\ln(k_2'(r,d_0))$ and $\ln(k_3'(r,d_0))$ vs $r-r_0$ in Figure 4, the correlations with distance for both the quenching and back electron transfer rate constants corrected for the contribution from the solvent reorganization energy are equally nondescript. The solvent correction does not significantly improve the distance correlations. By contrast, as shown in Figure 5, reasonably good linear correlations exist between $\ln(k_2'(d,d_0))$ and $d - d_0$ and between $\ln(k_3'(d,d_0))$ and $d - d_0$ for all four cases, $n = 2-5$. From the plots, in Figure 5, $\beta_2 = 0.41$ Å^{-1}, $k_2'(d_0) = 1.9 \times 10^9$ s^{-1} and $\beta_3 = 0.48$, $k_2'(d_0) = 1.7 \times 10^9$ s^{-1}. As noted earlier, with only four experimental points, the β values are not statistically defined. As shown by the solvent-uncorrected plots in Supporting Information Figure 4a,b, good correlations also exist between $\ln(k_2)$ and $d - d_0$ ($\beta_2 = 0.46$ Å^{-1}, $k_2(d_0) = 1.8 \times 10^9$ s^{-1}) and between $\ln(k_3)$ and $d - d_0$ ($\beta_3 = 0.46$ Å^{-1}, $k_2(d_0) = 1.7 \times 10^9$ s^{-1}).

Given the success of the correlations between $\ln(k_{ET}'(d - d_0))$ in Figure 5, there is no need to invoke a change in mechanism between $n = 2-4$ and $n = 5$. For example, the dominant mechanism for $n = 2-4$ could be through-bond or a chemical mechanism and, for $n = 5$, a through-space mechanism. The chemical mechanism for back electron transfer would involve a reduction of a proline spacer followed by proline-to-proline electron hopping; for example, for $n = 2$,

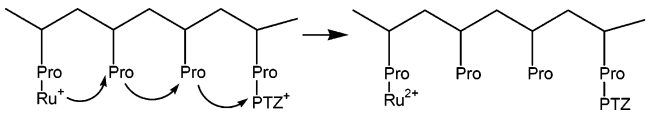

The success of the correlations with $d - d_0$ is provocative. It points to through-space electron transfer as the dominant electronic coupling mechanism in this series of oligoproline arrays. There may also be contributions from through-bond electron transfer, but through-bond electronic coupling appears not to be the dominant pathway for electron tunneling.

Electron Transfer in the Normal and Inverted Regions. The attenuation factors for thermally activated electron transfer in the normal region (k_2) and for activationless electron transfer in the inverted region (k_3) are essentially the same within experimental error. This is also a provocative and important observation since it points to the same electronic coupling mechanism for these fundamentally different processes.

Electron transfer for the two processes may involve different spin states. The initial MLCT excited "state" is actually a manifold of three closely spaced states, which are largely triplet in character. They arise from a lowest triplet state split by low symmetry and spin−orbit coupling.[30] Electron-transfer quenching occurs dominantly to give the spin-allowed triplet redox-separated (RS) state product,[29]

$$\underset{(^3\mathbf{MLCT})}{^3(Ru^{2+}*\text{-}(pro)_n\text{-}PTZ)} \rightarrow \underset{(\mathbf{RS})}{^3(Ru^{+}\text{-}(pro)_n\text{-}PTZ^{+})}$$

The ground state (GS), $^1(Ru^{2+}\text{-}(pro)_n\text{-}PTZ)$, is largely singlet in character, and, in principle, there is a spin prohibition to back electron transfer to give the ground state, $^1RS \rightarrow {}^1GS$. However, the splitting between the singlet and triplet states is expected to be very small, and anisotropic hyperfine coupling and electron spin−spin dipolar interactions provide mechanisms for their rapid interconversion.[31−33] Given the facts, interconversion followed by singlet → singlet electron transfer presumably dominate back electron transfer,

$$^3(Ru^+\text{-}(pro)_n\text{-}PTZ^+) \rightleftharpoons {}^1(Ru^+\text{-}(pro)_n\text{-}PTZ^+)$$
$$(^3\mathbf{RS}) \qquad (^1\mathbf{RS})$$

$$^1(Ru^{2+}*\text{-}(pro)_n\text{-}PTZ) \rightleftharpoons {}^1(Ru^+\text{-}(pro)_n\text{-}PTZ^+)$$
$$(^1\mathbf{RS}) \qquad (^1\mathbf{GS})$$

In the oligoprolines, both normal and inverted electron transfer are "non-adiabatic" in the sense that the electron-transfer coupling matrix element, H_{DA}, is small compared to the reorganization energy. In this regime, reaction dynamics and the frequency factor for electron transfer are dictated by weak electronic orbital overlap and the dynamics of electron tunneling.[18−23]

With strong donor−acceptor electronic coupling in the inverted region, as in excited-state nonradiative decay, the transferring electron is in equilibrium with the nuclear coordinates. "Electron transfer" becomes a transition between states, with the reaction dynamics dictated by nuclear motions that couple the initial and final electronic wave functions.[28,29,34] An example is nonradiative decay of MLCT excited states, e.g., $Ru^{III}(bpy^{\bullet-})(bpy)_2^{2+}* \rightarrow Ru^{II}(bpy)_3^{2+}$. In the $Ru^{II}(bpy)_3^{2+}*$ example, reaction dynamics and the frequency factor are dictated by vibronic coupling with a low-frequency Ru−N skeletal mode or modes that mix the excited and ground-state electronic wave functions.[28]

For adiabatic electron transfer in the normal region, reaction dynamics are dictated by the slowest coupled nuclear motion or motions. These are typically collective motions of the solvent that are coupled to the change in electronic distribution accompanying electron transfer.

Acknowledgment. This work was supported by the National Science Foundation under grant CHE-9705724 and the Department of Energy under research grant DE-FGO2-96ER 14607 (to T.J.M.). The authors thank Dr. Bassam Nakhle, Russ Henry, and Dr. A. Tripathi for help with this study and the NC Supercomputing Center for computing time.

Supporting Information Available: Computational programs, figures, MS and CD data. This material is available free of charge via the Internet at http://pubs.acs.org.

JA030659F

(30) Kober, E. M.; Meyer, T. J. *Inorg. Chem*. **1984**, *23*, 3877.
(31) Striplin, D. R.; McCafferty, D. G.; Wall, C. G.; Friesen, D. A.; Erickson, B. W.; Meyer, T. J. *J. Am. Chem. Soc*. **2004**, *126*, 5282−5291.
(32) Gilch, P.; Pöllinger-Dammer, F.; Musewald, C.; Steiner, U. E.; Michel-Beyerle, M. E. *Science* **1998**, *281*, 982.
(33) Klumpp, T.; Linsenmann, M.; Bürsserer, D.; Krissinel, E. B.; Larson, S. J.; Elliott, C. M.; Steiner, U. E. *J. Am. Chem. Soc*. **1999**, *121*, 1076.
(34) Demadis, K. D.; Hartshorn, C. M.; Meyer, T. J. *Chem. Rev*. **2001**, *101*, 2655.